Available online at www.sciencedirect.com
SCIENCE DIRECT®
Journal of Magnetic Resonance 174 (2005) 78–87
JMR Journal of Magnetic Resonance
www.elsevier.com/locate/jmr

An analytical methodology for magnetic field control in unilateral NMR

Andrew E. Marble [a,b], Igor V. Mastikhin [a,*], Bruce G. Colpitts [b], Bruce J. Balcom [a]

[a] MRI Centre, Department of Physics, P.O. Box 4400, University of New Brunswick, Fredericton, NB, Canada E3B 5A3
[b] Department of Electrical and Computer Engineering, P.O. Box 4400, University of New Brunswick, Fredericton, NB, Canada E3B 5A3

Received 1 November 2004; revised 7 January 2005

Abstract

Traditionally, unilateral NMR systems such as the NMR-MOUSE have used the fringe field between two bar magnets joined with a yoke in a 'U' geometry. This allows NMR signals to be acquired from a sensitive volume displaced from the magnets, permitting large samples to be investigated. The drawback of this approach is that the static field (B_0) generated in this configuration is inhomogeneous, and has a large, nonlinear, gradient. As a consequence, the sensitive volume of the instrument is both small and ill defined. Empirical redesign of the permanent magnet array producing the B_0 field has yielded instruments with magnetic field topologies acceptable for varying applications. The drawback of current approaches is the lack of formalism in the control of B_0. Rather than tailoring the magnet geometry to NMR investigations, measurements must be tailored to the available magnet geometry. In this work, we present a design procedure whereby the size, shape, field strength, homogeneity, and gradients in the sensitive spot of a unilateral NMR sensor can be controlled. Our design uses high permeability pole pieces, shaped according to the contours of an analytical expression, to control B_0, allowing unilateral NMR instruments to be designed to generate a controlled static field topology. We discuss the approach in the context of previously published design techniques, and explain the advantages inherent in our strategy as compared to other optimization methods. We detail the design, simulation, and construction of a unilateral magnet array using our approach. It is shown that the fabricated array exhibits a B_0 topology consistent with the design. The utility of the design is demonstrated in a sample nondestructive testing application. Our design methodology is general, and defines a class of unilateral permanent magnet arrays in which the strength and shape of B_0 within the sensitive volume can be controlled.

Keywords: Unilateral NMR; Nondestructive testing; Inhomogeneous fields; Pole pieces; Magnet design; NMR-MOUSE

1. Introduction

In a conventional nuclear magnetic resonance (NMR) experiment, the sample under study is placed in a homogeneous magnetic field produced by a superconducting solenoid. While this facilitates high signal-to-noise, geometrically correct, spatially resolved magnetic resonance imaging (MRI), it limits the range of samples that can be examined. In recent years, this limitation has been addressed by the introduction of 'inside out' or unilateral NMR [1–6]. In this methodology, the fringe field from a permanent magnet array is used to generate the B_0 field in a volume displaced from the device. A surface coil or an alternate RF probe geometry is used to generate a remote B_1 field. The shapes of these inhomogeneous fields define a 'sensitive volume' or 'sensitive spot' where components of the two fields are orthogonal. Designs of this type allow near surface measurements to be made on samples of arbitrary sizes previously inaccessible to NMR. Furthermore, small

* Corresponding author. Fax: +1 506 453 4581.
E-mail address: mast@unb.ca (I.V. Mastikhin).

1090-7807/$ - see front matter © 2005 Elsevier Inc. All rights reserved.
doi:10.1016/j.jmr.2005.01.009

permanent magnet designs are easily transported, making them suitable for field applications. The strong gradient inherent in these designs can be exploited to investigate slowly diffusing samples [7], or to suppress the signal from rapidly diffusing samples [8].

Inside-out NMR was first used in the oil industry for well logging [1–3]. Later, Eidmann et al. [4] developed a portable unilateral NMR sensor known as the NMR-MOUSE. This design employs a 'U' magnet geometry in which two permanent magnets are arranged on a ferromagnetic yoke in opposite orientations with a gap between them. The B_0 field curls between the two magnets, giving a component parallel to their faces in the area over the gap. A surface coil in the gap with its axis normal to the face of the magnets provides the B_1 field. While this type of design has been successfully employed in a variety of NMR studies [9–12], significant drawbacks exist. The B_0 field provided by the magnet array is inhomogeneous in all directions and suffers from a strong (10–50 T/m [8]), nonlinear gradient in the direction normal to the array. This results in short signal lifetimes, obscuring chemical shift information and resulting in low SNR measurements. The strong nonlinearity of the gradients results in an ill-defined sensitive volume precluding conventional spatially resolved measurements. The strong gradient causes every RF excitation to be slice selective; the size, shape, and position of the excited volume are determined by the bandwidth and frequency of the RF pulse sequence used. These effects limit the effective resolution of the sensor by obscuring the location and distribution of the spin population observed in a measurement. The strong gradient also requires additional RF circuitry to be employed in order to vary the excitation frequency over a wider range in spatially resolved measurements [13].

To address the drawbacks of early unilateral NMR systems, several new designs have been proposed. Using a single bar magnet to provide B_0, Blümich et al. [5] developed a unilateral sensor with a small volume directly over one of the poles of the magnet. In this volume, the gradient parallel to the magnet face is negligible while the gradient normal to the magnet face is strong but approximately linear. While this design offers some advantages in certain applications, the B_0 field is orthogonal to the face of the magnet, excluding the use of a simple surface coil to generate B_1. Specially designed planar coils must be used, resulting in a decrease in sensitivity.

Many other designs exist wherein the position of magnets in an array is modified in order to achieve some desirable characteristic in the topology of B_0 [14,15]. The common feature of these designs is that all deal with a forward problem: given a particular magnet array, determine the resulting B_0 field and subsequently determine how this field topology can be applied to achieve experimental goals. This paper seeks to answer the inverse problem: given an experimental goal, select an appropriate B_0 topology, and synthesize a design for an instrument providing this field.

Methods of simulating the B_0 field due to a given arrangement of magnets exist, for example, the finite element (FEM) approximation. Designs can be optimized by performing successive simulations while varying parameters to minimize some goal function and this technique has previously been employed in unilateral magnet design [16]. The drawback of this approach is that specific parameters (e.g., size, position, and strength of magnets) must be selected for the optimization and the parameter space must be empirically selected to suit the desired magnet topology. Furthermore, conventional simulation techniques are computationally expensive, leading to long optimization times, and constraining the number of parameters that can be optimized. Our technique synthesizes a unilateral magnet array based on a simple analytical expression and does not, in principle, require any a priori knowledge of the desired magnet geometry.

To accomplish this synthesis, we have considered the addition of high permeability material above the magnet array. This approach is standard in the design of closed permanent magnet NMR systems, where high permeability 'pole pieces' are used to control B_0 between the magnets. Many methods of shaping the pole pieces to provide an optimal B_0 topology have been proposed [17–20], however, all deal with generating a homogeneous field between two magnets and cannot be directly applied to the unilateral case. Glover et al. [20] recently presented a permanent magnet-based 1D profiling system in which pole pieces, shaped according to contours of magnetic scalar potential, were used to give a desired static field. This approach is attractive in that it offers a low complexity method of configuring magnets and pole pieces to control B_0. To extend this work to the unilateral design regime, we have developed a design methodology wherein a planar array of magnets are fitted with pole pieces shaped according to a linear combination of solutions to Laplace's equation. These shapes correspond to equipotential contours of magnetic scalar potential. Our technique allows the size, shape, and gradient of a sensitive spot displaced from the array to be controlled. The accuracy of the field topology generated by the array is commensurate with the order of the solution.

In this work, we present the proposed design methodology, and detail the construction of a prototype unilateral array with a controlled sensitive volume. This array was designed to maximize the magnetic field homogeneity in the sensitive spot in order to maximize the NMR signal in a nondestructive testing application. It is shown that the prototype array has a B_0 topology consistent with that determined analytically through our design method. Finite element simulation results are presented, elucidating differences between the calculated

and measured B_0 fields. These differences, although minor, result from the approximations used in the solution.

The functionality and improved performance of the fabricated array are demonstrated through a series of test measurements. Diffusion measurements, used to calculate the homogeneity of the sensitive volume show a gradient of 0.13 T/m, orders of magnitude below that observed in many inside out NMR devices [5,6,8], and on par with carefully optimized unilateral well-logging instruments [2]. The utility of the new design is demonstrated through nondestructive evaluation of moisture ingress in an epoxy metal composite sandwich panel. The fabricated array represents a preliminary application of our design technique. In general, this technique allows a magnet array to be designed to approximate any given field topology. The accuracy of the approximation is limited by the complexity of the design and the strengths of the magnetic materials available.

2. Theory

A static magnetic field vector, $\vec{B}$, can be described in terms of a magnetic scalar potential, ϕ, as

$$\vec{B} = \nabla\phi. \tag{1}$$

Since magnetic fields do not diverge, the divergence of Eq. (1) gives Laplace's equation,

$$\nabla^2\phi = 0, \tag{2}$$

the solution of which is well known. Our design uses contours of ϕ in the z–y plane, extended along the x-axis, and thus we consider only the two-dimensional solution to Laplace's equation. In two dimensions, by writing ϕ as the product of two one-dimensional functions, we select the particular solution

$$\phi(z,y) = \mathrm{e}^{-ay}[b\cos(az) + c\sin(az)], \tag{3}$$

where a, b, and c are arbitrary constants. Because the Laplacian operation is linear, a linear combination of solutions of the form of Eq. (3) will also satisfy Eq. (2). For our application, it is desired that the magnetic field be parallel to the plane of the magnet array. It follows that the magnetic potential should be an odd function with respect to the center of the array, allowing the field to curl from one side to the other. Accordingly, we set b to zero and write ϕ as

$$\phi(z,y) = \sum_{i=0}^{N-1} \mathrm{e}^{-a_i y} c_i \sin(a_i z). \tag{4}$$

The magnetic field due to the potential described by Eq. (4) can be calculated using Eq. (1), resulting in

$$\begin{aligned}\vec{B} &= \frac{\partial\phi}{\partial z}\hat{z} + \frac{\partial\phi}{\mathrm{d}y}\hat{y} \\ &= \sum_{i=0}^{N-1} a_i c_i \mathrm{e}^{-a_i y}[\cos(a_i z)\hat{z} - \sin(a_i z)\hat{y}].\end{aligned} \tag{5}$$

For an Nth order design, the parameter vectors $A = [a_0\ a_1 \cdots a_{N-1}]$ and $C = [c_0\ c_1 \cdots c_{N-1}]$ can be selected to approximate a desired $\vec{B}$ over a region of interest (ROI). Sample calculations and finite element simulations have shown that larger values of N will result in better control of $\vec{B}$, at the cost of design complexity.

Following Glover et al. [20], the surface of a high permeability ($\mu_r \gg 1$), linear, isotropic material can be approximated as an equipotential contour of ϕ. Thus, a potential described by Eq. (4) can be realized using pole caps shaped according to the contours of $\phi =$ constant, mounted on permanent magnets of an appropriately chosen strength. This design strategy defines a family of magnet arrays suitable for unilateral NMR applications. The two-dimensional designs can be realized in 3D by making the magnets and pole caps sufficiently long in the x-direction such that edge effects are not present over the center of the array. Several approximations are used in our design procedure. As previously stated, the effects of the finite length of the array in the x-direction have been neglected. This is common practice in unilateral NMR magnet design although its ramifications are rarely discussed in the literature. The analytical design also assumes that ϕ is periodic in the z-direction. In a practical implementation, the scalar potential becomes truncated due to the finite size of the magnet array. Simulations have indicated that B_0 can be controlled for y and z close to the array in a design of finite size. The effects of the approximations used will be considered in a future publication.

3. Design example

Here, we illustrate the utility of the technique, specifically the ability to tailor a magnet geometry to a specific application. The theory described above was used to design a unilateral sensor for the detection of moisture ingress into graphite/aluminum/epoxy composite sandwich panels. The primary design goals for this magnet array were: (1) a large sensitive volume to combat the poor SNR inherent in this sample; (2) a low resonant frequency to mitigate interactions between B_1 and the conductors in this structure. For a description of the composite sandwich panel and the challenges associated with the application of NMR to this sample, see [21].

3.1. Problem definition

From Eq. (3), it is clear that any units of length can be chosen for the design, and thus the magnet array can be designed in arbitrary units and scaled to a desired size as appropriate. In this example, the solution space has a width of approximately d units. The ROI is $0.275d$ units above the plane of the magnets and centered over the array. It is $0.25d$ units in width and $0.1d$

units in height. Within the ROI, it is desired that |B|, the modulus of $\vec{B}$, should be constant, giving a constant resonant frequency, ω_0, inside this volume. To achieve the desired field within the ROI, a cost function was developed. In this example, the deviation of |B| from its mean value over the ROI was minimized. The resulting design goal can be represented mathematically by

$$\min_{A,C} \iint_{\mathrm{ROI}} (|B| - |\bar{B}|)^2 \,\mathrm{d}z\,\mathrm{d}y, \tag{6}$$

where $|\bar{B}|$ is the average modulus of $\vec{B}$ over the ROI. Although this was the minimization criteria used, it suffers the notable disadvantage of having the trivial solutions $a_i = 0$ and $c_i = 0$, necessitating that a_0 and c_0 be fixed. However, there are advantages in fixing a_i, and fixing c_0 will simply have a scaling effect on the solution. Thus, Eq. (6) is equivalent to evaluating

$$\min_{A,C} \iint_{\mathrm{ROI}} (|B| - D)^2 \,\mathrm{d}z\,\mathrm{d}y,$$

for some constant D. The exact function to be minimized is dependent on the desired field configuration. For example, if it was desired that B had no y-component and a constant gradient, G, in the y-direction centered about y_0, the minimization problem could be

$$\min_{A,C} \iint_{\mathrm{ROI}} \left[(B_z - (D + G(y - y_0)))^2 + (B_y - 0)^2 \right] \mathrm{d}z\,\mathrm{d}y. \tag{7}$$

The cost function given in Eq. (6) was evaluated to determine the optimal parameters for $N = 3$. This order was selected as a compromise between accurate control of B_0 and complexity of the resulting magnet array. To better define the problem, values were selected for the parameter vector A. The terms, a_i are arguments of the sine function in Eq. (4) and thus represent spatial frequencies present in the scalar potential. It thus makes sense to include frequencies describing large scale variations across the array geometry, as well as higher frequencies describing local detail within the pole caps. Accordingly, a_0 is selected to correspond to a 'fundamental' frequency, $a_0 = 2\pi/\mathrm{d}$. In this example, subsequent values of a_i were set to $a_1 = (4/3)\pi/\mathrm{d}$ and $a_2 = \pi/\mathrm{d}$. These three frequencies cover a relatively narrow range of detail in the shape of the pole pieces and were selected as a compromise between design complexity and accurate approximation of the desired field. In principle, these values need not be specified and appropriate parameters will arise naturally as a result of the optimization. In this case, it would have been necessary to modify the goal function in order to ensure that the optimal ϕ could be realized with a unilateral design.

With A set, the optimal value of C was determined by minimizing the cost function over a discrete solution space using the Matlab optimization toolbox. The parameter c_0 was fixed in order to avoid a trivial solution in the optimization. Fig. 1 shows a contour plot of the scalar potential resulting from the optimization of the remaining parameters. The ROI is indicated by the dashed box. The thick solid lines represent the contour lines selected as pole pieces. The selected contours are as close to the ROI as possible as the magnetic field will always decay rapidly with distance from the magnets. The magnitude of ϕ for the inner two contours is 1/7 the magnitude for the outer contours. The sign of ϕ alternates between positive and negative for each of the poles. It is important to note that the number of pole pieces was not specified in order to achieve the design. The shape of the contours is solely the result of minimizing Eq. (6) with the constraints discussed.

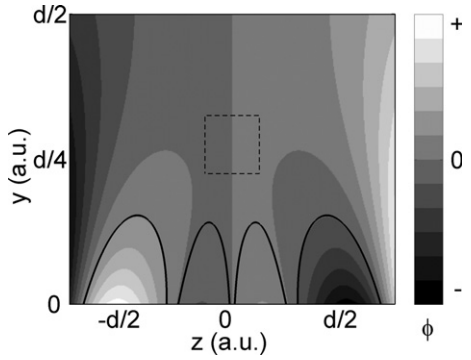

Fig. 1. Contour plot of the optimized magnetic scalar potential for our design, given by Eq. (4). The target sensitive volume is indicated by the dashed box. Equipotential contours of ϕ, close to, but below the sensitive volume, are selected to define the shape of the pole pieces. The contours selected for our design are shown by the solid lines. The design takes place in unitless dimensions, allowing it to be arbitrarily scaled.

Taking the gradient of ϕ gives the magnetic field strength, B. Fig. 2 gives a contour plot of the x-component of the field, B_x, due to the scalar potential depicted in Fig. 1. Here, the solution has been scaled such that the distance between the opposite edges of the outer pole caps is 15 cm (6 in.). The contours are given in percent as the absolute field strength will depend on the strength magnets used in the design. It is observed that the spatial variation of B_x within the ROI is at a minimum. At the center of the ROI, the field gradient is zero. In the calculated solution, B_x increases in magnitude as y increases. This occurs because the calculation assumes that ϕ can be controlled everywhere. In a practical implementation, B_0 must always eventually fall off with distance from the magnets. It will be shown, however, that near the array, the shape of B_0 is readily controlled using the pole caps.

3.2. Array construction

Using the contours shown in Fig. 1, a four-magnet array was constructed. The geometry of the array is de-

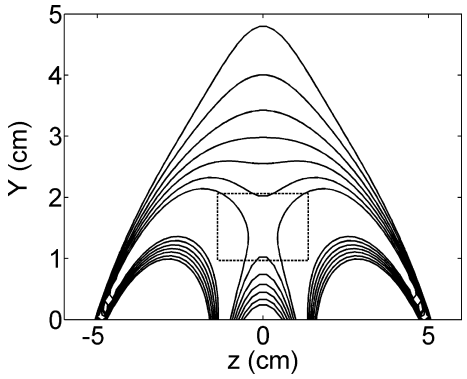

Fig. 2. Contour plot of the z-component of the theoretical magnetic field for our design, determined analytically as the gradient of the scalar potential field shown in Fig. 1. The target sensitive volume is denoted by the dashed box. The position, $y = 0$, corresponds to the surface of the inner pole pieces. The field contours represent an 8% change in the magnetic field strength. The actual field strength is dependent on the strengths of the magnets used in the construction. It is observed that there is a saddle point at the center of the target sensitive volume.

picted in Fig. 3. The outer magnets were 5 cm (2 in.) in height and 4 cm (1.7 in.) in width, while the inner magnets were 2.5 cm (1 in.) wide. The entire array was 15 cm (6 in.) wide, and was made to be 15 cm (6 in.) long in the x-direction.

NdFeB magnets, manufactured by the Yuxiang Magnetic Materials Ind., provide the B_0 field. Due to manufacturing restrictions, the magnets were all manufactured with a surface magnetic field of 0.5 T. As noted earlier, the analytical design specified that ϕ at the inner pole pieces was to be 1/7 that at the outer pieces and ideally, the relative strengths of the magnets would have been scaled to reflect this. Because high field permanent magnets must be fully saturated, manufacturing them to different strengths is difficult. In the future, the possibility of varying the thickness of the magnets (in the y-direction) to achieve the desired relationship between their strengths will be explored. Because the relative strengths of the magnets differed from those specified in the design, the position of the sensitive spot and the magnitude of B_0 were altered from those in the analytical design in a predictable way. This will be considered further in Section 3.3.

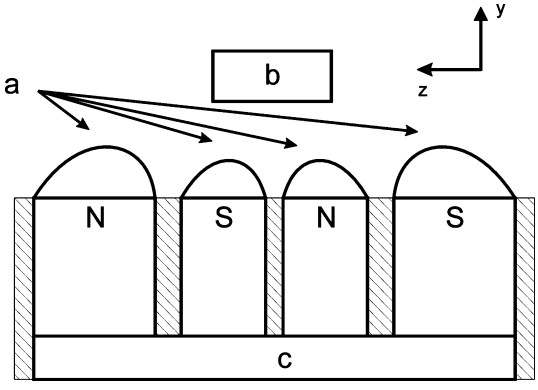

Fig. 3. Diagram of the fabricated array. The pole pieces (a) rest over the permanent magnets, whose relative field directions (North/South) are indicated in the figure. The target sensitive volume is highlighted by the box (b). The area (c) is an iron yoke, used to concentrate and contain the magnetic field on the bottom of the array. The hatched area represents the aluminum structure used to house the magnets. The pole pieces are bolted to the aluminum at either end.

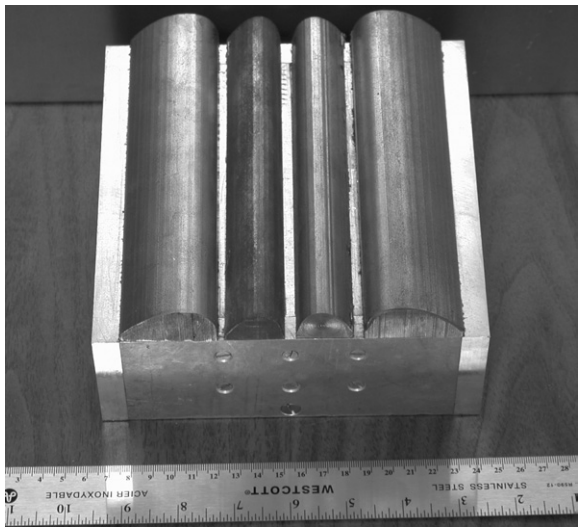

Fig. 4. Photograph of the constructed array, including a distance scale. The yoke (not visible) is attached below the magnets. The pole pieces are machined from high permeability steel. The four NdFeB magnets are housed under the pole pieces. Each has a surface field strength of 0.5 T.

The magnets were housed in an aluminum frame with an iron yoke concentrating the field at the bottom of the array. To safely place the magnets in the frame, 0.95 cm (3/8 in.) holes were drilled through the yoke under the slot for each magnet. The holes were tapped allowing nonmagnetic threaded rod to be fed through them. A guiding structure was then built to fit over the frame, allowing each magnet to be inserted in turn away from the others. By turning the threaded rod back out of the frame, the magnets were slowly lowered into position in a controlled manner.

The pole pieces were machined from high permeability steel using a 3-axis ES-V4020 CNC vertical machining center. Threaded holes were drilled in the flat face of the pole pieces, allowing them to be bolted up through the aluminum frame. Nonmagnetic brass screws were used in all aspects of the construction. Fig. 4 shows a photograph of the array.

3.3. Design validation

To compensate for the differences between the analytical design and the manufactured array, the array was simulated using the FEMLAB finite element simulation

software. Magnetic fields in y–z plane were evaluated assuming the array was infinite in the x-direction. Fig. 5 shows a simulated contour plot of the z-component of B_0. The field strength is expressed as contours of the resonant frequency for ^{1}H. The position $y = 0$ corresponds to the upper surface of the inner pair of pole pieces. Only the z-component is presented as this is the main component of B_0 and is readily compared to measurements from the fabricated array using a 1-axis gaussmeter.

It is immediately apparent that the simulation results agree with the analytically determined field topology presented in Fig. 2. The saddle point in the field is present but is displaced due to changes in the relative strengths of the magnets. For large values of y and z, there is a deviation between the analytical and simulated results as the analytical results assume that ϕ can be controlled everywhere.

Using a Lakeshore 450 1-axis gaussmeter, the z-component of the magnetic field from the fabricated array was measured over the center of the x-dimension of the magnets on a 1 cm grid. A plot of the measured magnetic field, presented as ^{1}H frequency contours, is shown in Fig. 6. The overall distribution of field lines in the plot is consistent with that presented for the simulated array. The sensitive volume is indicated by the saddle point in the plot. It is ~1.5 cm in width and ~1.5 cm in height and is centered about 2 cm up from the inner pole pieces. There is a slight difference between the position of the sensitive spot in the measured and simulated results. This systematic difference is attributed to the combined effects of differences between the actual and simulated magnetic fields for the magnets, along with a small change in the height of the manufactured pole pieces, introduced to facilitate their fabrication.

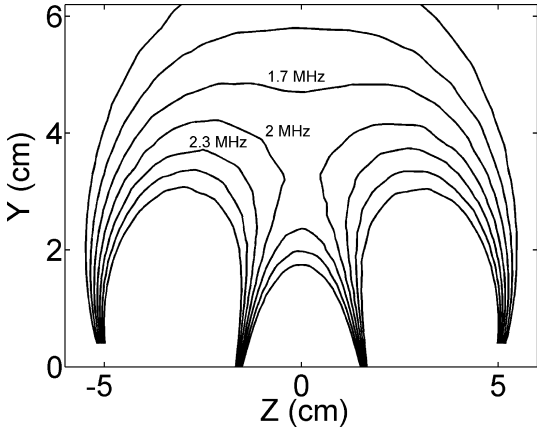

Fig. 5. Simulated magnetic field (B_z) contour plot for the array. The field contours are labeled in MHz for ^{1}H magnetic resonance according to the Larmor equation. The distance, y, is measured from the upper surface of the inner set of pole pieces. The shape of the simulated field is clearly similar to that predicted by the analytical expression. The saddle point in the magnetic field strength is again present over the center of the array, however, it is displaced in the y-direction due to differences between the magnets used in fabrication and those specified in the design. At large (y,z), the field topology deviates from its predicted shape because of the finite dimensions of the array.

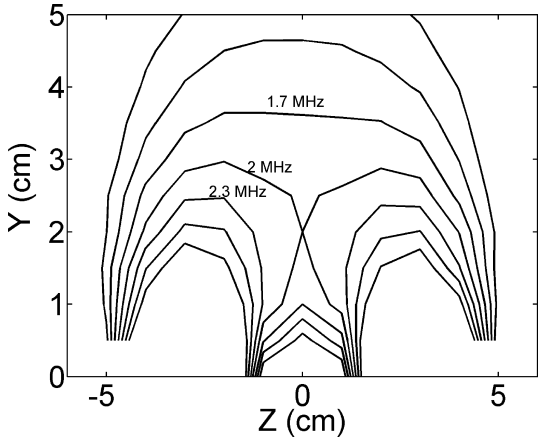

Fig. 6. Measured magnetic field contour plot for the array. The field contours are labeled in MHz for ^{1}H magnetic resonance according to the Larmor equation. The result is in congruence with the simulated result in Fig. 4. The distance, y, is measured from the upper surface of the inner set of pole pieces. The observed shift in the position of the sensitive volume is attributed to differences between the fabricated and simulated magnets and pole pieces, along with inaccuracies in the field measurement introduced by errors in the position and orientation of the hall sensor.

4. Experimental results

In this section, several sample NMR measurements using the prototype array are presented, illustrating the performance of the device. In each case, the resonant frequency was 2.01 MHz and a 10 turn, capacitively coupled, 2 cm diameter surface coil positioned above the array was used for the measurements. The coil quality factor was approximately 27. The size of the surface coil limits the size of the sensitive volume in the x-direction, while the dimensions of the homogeneous region of B_0 limit the volume in the y–z plane.

4.1. NMR signal characteristics

Fig. 7 shows a test measurement made with the array. The solid line represents the peak magnitudes for the first 32 echoes in a phase cycled CPMG sequence using a polyisoprene rubber sample larger than the sensitive volume selected by the coil. The dashed line represents the noise level for the system. It is observed that there is a large amount of noise present in the acquisition. This is attributed to the open design of the array along with the low acquisition frequency. The observed decay constant was 3.3 ms.

Fig. 8 compares single echoes acquired with a α–τ–2α–τ pulse sequence. The solid line shows an echo acquired from a polyisoprene sample using the

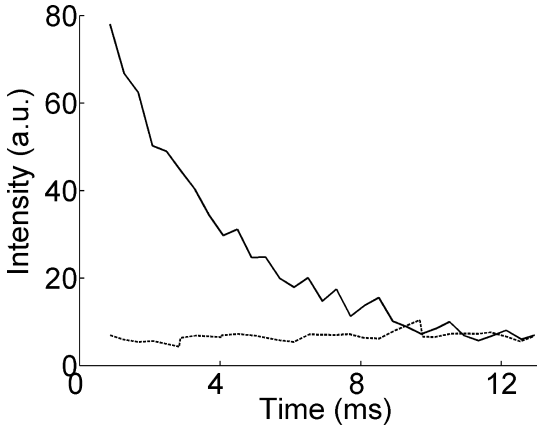

Fig. 7. Observed CPMG decay (solid line) for a polyisoprene rubber sample measured at 2.01 MHz with the fabricated array. The echo time was 0.4 ms. Thirty-two echoes were acquired with 512 averages. A nominal 90° pulse length of 2 μs, along with a corresponding 180° pulse of 4 μs was used in the acquisition. The observed decay constant was $T_{2\text{eff}} = 3.3$ ms. The T_2 of the polyisoprene sample was 1.4 ms at 8.3 MHz. Differences between these values are attributed to the change in B_0 strength, as well as a slight spin-locking effect brought on by the inhomogeneous field and short echo time. The dashed line shows the noise level in a measurement made with no sample present. The observed noise in the measurement is high due to the low frequency and open design of the array.

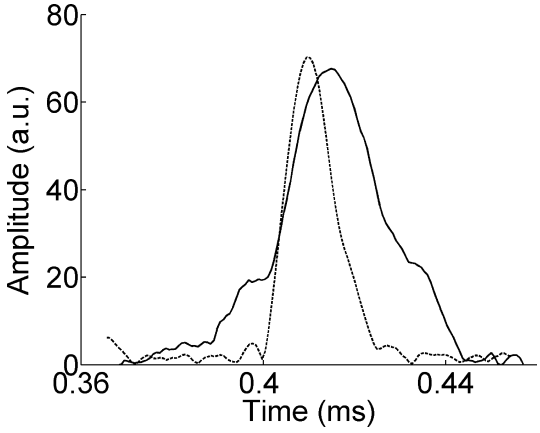

Fig. 8. Comparison between spin echoes observed using our array at 2.01 MHz (solid line) and a commercial unilateral NMR sensor at 14.85 MHz (dashed line). Both measurements were made on a polyisoprene sample larger than the sensitive volume of the devices. The echo time was 0.4 ms and 512 scans were used. Both measurements exhibit comparable SNRs. The echo for the prototype array is broader than that for the commercial instrument, although the excitation bandwidth is broader.

prototype array while the dotted line shows an echo acquired from the same sample using a commercial MOUSE system operating at 14.85 MHz using a 1 cm diameter, one turn surface coil with a quality factor of approximately 80. For the commercial system, the size of the sensitive volume was completely limited by the homogeneity of B_0, rather than the geometry of the RF coil. The nominal 90° and 180° pulse widths for the array measurement were 2 and 4 μs, respectively. For the MOUSE measurement, the pulse width was fixed at 6 μs and the amplitude was adjusted to achieve the appropriate flip angles. All other experimental parameters for both measurements were identical.

It is observed that both echoes shown in Fig. 8 have comparable SNR levels. This indicates that the increase in the size of the sensitive volume resulting from the controlled B_0 field in our array, along with the coil design, compensates for any SNR disadvantages due to the lower operating frequency [22]. It is expected that optimization of the coil design would result in a substantial increase in SNR.

The echo observed from the array is also much broader than that from the MOUSE. The observed T_2^* is on the order of 10's of μs, indicating broadband excitation from the short RF pulse. In a strongly inhomogeneous static field, the observed signal lifetime is approximately equal to the duration of the RF pulse due to the wide range of precession frequencies of the excited spins. This is true for the MOUSE measurement, however, despite the shorter pulses used with our array, the signal lifetime is much longer. The 'shoulders' observed on the echo from our array have been observed elsewhere in measurements and simulation at comparable magnetic field strengths and homogeneities [23].

4.2. Field inhomogeneity measurement

Measurements on diffusive samples were made in order to quantitatively assess the homogeneity of the B_0 field for the prototype array. Using a doped water sample larger than the instrument sensitive volume, the effects of diffusive attenuation on a CPMG measurement were examined for the array. A CPMG decay for this sample obtained with the array is presented in Fig. 9. The observed decay constant is 45 ms, in agreement with the sample T_2, indicating that diffusive attenuation has a negligible effect on this measurement. Identical measurements made with the commercial unilateral sensor showed a decay constant of 1.3 ms, clearly the result of diffusive attenuation brought on by the strong gradient associated with this device. While this is desirable in some applications [8], the advantage in observing fast-diffusing systems is clear. The observed decay constants for the doped water and the polyisoprene sample were slightly longer than the sample T_2 values measured at 8.3 MHz. This is attributed to the contribution of $T_{1\rho}$, the sample spin-lock relaxation constant, and T_1, the spin–lattice relaxation time, due to the inhomogeneity of B_0 [24]. Furthermore, the difference in frequency could have an effect on the sample T_2. Since diffusive attenuation is irreversible, the effects of $T_{1\rho}$ and T_1 do not enter in to comparisons concerning this effect. Clearly, the decreased sensitivity to diffusion exhibited by our prototype represents a tremendous

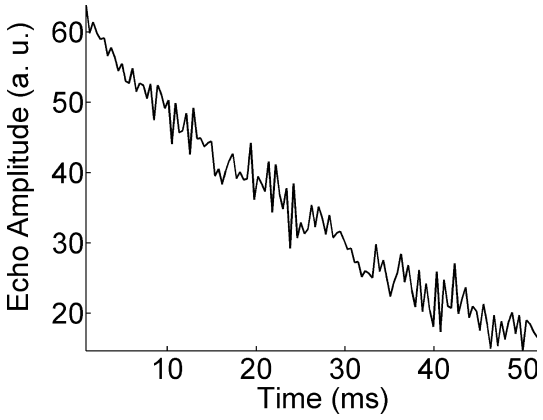

Fig. 9. CPMG measurement of a liquid sample using our array. The sample was a bottle of doped water ($T_2 = 36.2$ ms at 8.3 MHz) much larger than the sensitive volume of the device. The echo time was 0.4 ms and 512 scans were averaged. The observed relaxation constant was 45 ms, indicating that the effects of diffusion were negligible. A signal lifetime of <2 ms was observed for the same measurement using a commercial unilateral NMR sensor. The discrepancy between the observed relaxation constant and the sample T_2 results from a combination of spin-locking effects and the difference in frequency.

advantage in measuring rapidly diffusing samples, and alludes to the homogeneity of B_0.

To quantify this homogeneity, the effects of diffusive attenuation on the signal from a distilled water sample larger than the sensitive volume were measured using the array while the echo time was varied. Assuming that the sample has a T_2 that is much longer than the decay constant due to diffusion, the observed decay constant for a CPMG measurement is given by Callaghan [22] as

$$\frac{1}{T_{2\text{eff}}} = \frac{\gamma^2 D}{3} G^2 \tau^2. \tag{8}$$

Varying τ and plotting the inverse of the effective decay constant against τ^2 results in a straight line with a slope related to the gradient, G, in B_0. Fig. 10 shows such a plot measured using the array for τ values between 1 and 4 ms. The slope of the line is 1.03×10^6 s^3. Assuming the diffusion constant of distilled water to be 2.51×10^{-9} m^2/s at room temperature [25], the calculated gradient is 0.13 T/m.

4.3. Moisture detection in composite panels

The motivation behind the development of this prototype was the detection of moisture within composite sandwich panels. Because of the difficulties associated with this type of sample, our measurements using conventional unilateral NMR devices have previously yielded unacceptable results. To validate the prototype array, measurements were made of a representative composite test sample. The sample, described in detail in [21], consisted of a 4 cm × 4 cm sandwich panel, 16 mm in thickness. The panel had an anodized alumi-

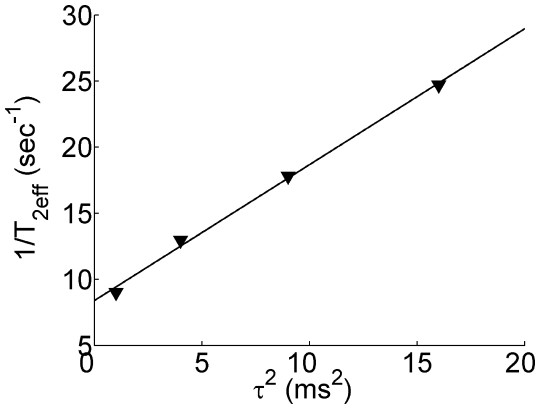

Fig. 10. Plot of the inverse of the observed decay constant against the echo time squared for a series of CPMG measurements made using our array at various echo times for a distilled water sample. Assuming that the decay is dominated by diffusive attenuation, the slope of the line can be related to the gradient in B_0. Taking the diffusion constant of water to be 2.51×10^{-9} m^2/s, the gradient is calculated to be 0.13 T/m.

num honeycomb core sandwiched between graphite epoxy composite skins. Ten central cells of the honeycomb lattice were partially filled with a total of ~2 mL of doped water. The goal of the moisture detection was to see a clear NMR signal from the water within the cells despite the shielding effects of the graphite skin and aluminum core.

Fig. 11 shows the signal observed from the water with the prototype array. The CPMG decay is both strong and relatively long lived. This is a combination of the larger sensitive spot and better field homogeneity of the array, as well as the lower frequency of the RF field. The low frequency of our prototype permits RF penetration of the graphite skin. This results in a successful

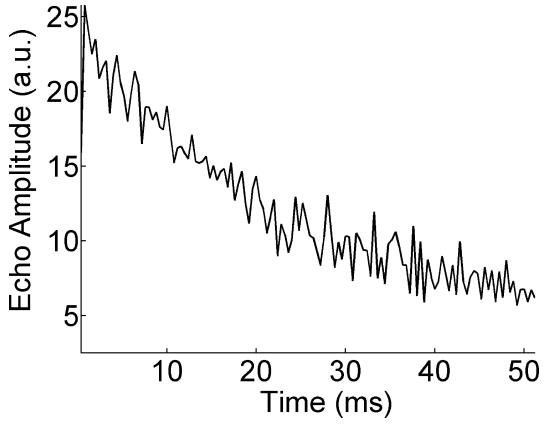

Fig. 11. CPMG measurement of water inside of a representative sample of aluminum/epoxy/graphite composite. Ten cells inside a 4 cm × 4 cm composite sample were filled with approximately 2 mL (total) doped water for this measurement. The prototype, with an echo time of 0.4 ms and 512 scans, yields a strong and readily interpretable result. This is attributed to the larger sensitive volume, a better field homogeneity and the lower RF frequency, allowing better B_1 penetration through the conductive skin.

measurement which was not possible with the commercial MOUSE due to its higher frequency of operation.

5. Conclusions

A methodology for the design of a new class of unilateral NMR instrument has been presented. By shaping high permeability pole pieces based on contours of an analytically derived expression for the magnetic scalar potential, it becomes possible to control the magnetic field topology in a region displaced from an array of magnets. This methodology is quite general and leads naturally to a family of planar arrays with displaced sensitive volumes. By optimizing a simple expression for the magnetic field in the sensitive volume, it is possible to control the orientation, magnitude, gradients, and homogeneity of the B_0 field in this region.

Through the design and construction of a prototype magnet array, the design methodology has been demonstrated to work, with the B_0 field of the fabricated array exhibiting close agreement with that specified in the design. Sample measurements show the prototype instrument obtains a field homogeneity of 0.13 T/m in the sensitive volume, on par with other optimal designs of this type [2,16]. The field strength for the design presented is lower than that often used is unilateral systems such as the NMR MOUSE. While the increased field homogeneity is partially a consequence of this lower field strength, the design idea presented here provides a simple way of controlling and optimizing the magnetic field homogeneity of a unilateral NMR instrument. The tradeoffs between field strength and homogeneity are the subject of ongoing research.

The utility of our design has been demonstrated in its application to a nondestructive testing problem of aerospace interest. It has been shown that the large, homogeneous sensitive volume of our instrument is suitable for the detection of water within composite sandwich panels.

Devices of this type can be tailored to specific magnetic resonance applications. Using this design methodology, we intend to develop a family of unilateral sensors suited to a range of NMR investigations.

6. Experimental

Optimization of Eq. (5) used the Nelder–Mead simplex method [26], implemented in the Matlab (The Mathworks, Natick, MA) software package. Finite element simulations used the FEMLAB (Comsol, Burlington, MA) package. The relative magnetic permeability of the NdFeB magnets was assumed to be 1.05; that of the iron yoke, as well as that of the pole pieces was assumed to be 100. The permeability of the aluminum frame was not considered. The simulation used 14,483 mesh nodes.

The commercial unilateral NMR system used was a Bruker (Rheinstetten, Germany) MOUSE, driven by a Minispec mq Series console running Minispec V2.41 software. The resonant frequency was 14.85 MHz, resulting in the selection of a $\sim$5 mm $\times$ 5 mm $\times$ $\sim$1 mm sensitive volume displaced 5 mm from the surface of the MOUSE. The RF amplifier was rated for 300 W. A Bruker surface coil was used for all measurements. The nominal pulse width of 6 μs was selected by varying the pulse width to maximize the echo amplitude in a spin echo measurement.

The low ^{1}H frequency for the prototype array precluded the use of the Bruker console alone for acquisition. The Bruker Minispec software and pulse programming hardware were used, however, the Minispec amplifier was replaced with an Amplifier Research (Bothell, Washington) 200 L 300 W broadband amplifer. A preamplifier built around a Miteq (Hauppauge, NY) RF amplifier was used in detection. The amplifier did not allow amplitude control to be programmed and thus different 90° and 180° pulse lengths were required. Pulse lengths of 2 and 4 μs, respectively, were selected by maximizing the amplitude of an observed spin echo. For the sandwich panel measurements, these values were modified to 3 and 6 μs. All measurements used a 10 turn 2 cm diameter capacitively coupled surface coil. The resonant frequency was 2.01 MHz.

The doped water samples used Gadolinium Chloride as the doping agent and had a measured T_2 of 36.2 ms at 8.3 MHz. The polyisoprene sample had a measured T_2 of 1.3 ms at 8.3 MHz. These measurements were performed in the homogeneous magnetic field of a permanent magnet system with a 14 cm pole gap.

Acknowledgments

We thank the Canadian Department of National Defence for related funding. A.E.M. thanks NSERC for financial assistance (PGSM) in addition to the New Brunswick Innovation Foundation. B.J.B. and I.V.M. thank NSERC for Discovery grants. B.J.B. thanks NSERC for an equipment grant for the Minispec and MOUSE instruments. B.J.B. also thanks the Canada Chairs program for a Research Chair in MRI of materials (2002–2009). The UNB MRI Centre is supported by an NSERC Major Facilities Access Award. We thank Rod MacGregor for technical assistance and Trevor DesRoches for his expert work in machining the pole pieces.

References

[1] R.K. Cooper, J.A. Jackson, Remote (inside-out) NMR. I. Remote production of region of homogeneous magnetic field, J. Magn. Res. 41 (1980) 400–405.

[2] R.L. Kleinberg, A. Sezginer, D.D. Griffin, M. Fukuhara, Novel NMR apparatus for investigating an external sample, J. Magn. Res. 97 (1992) 466–485.
[3] D. Allen, S. Crary, B. Freedman, M. Andreani, W. Klopf, R. Badry, C. Flaum, B. Kenyon, R. Kleinberg, P. Gossenberg, J. Horkowitz, D. Logan, J. Singer, J. White, How to use borehole nuclear magnetic resonance, Oilfield Review, Summer (1997) 34–57.
[4] G. Eidmann, R. Savelsberg, P. Blümler, B. Blümich, The NMR MOUSE, a mobile universal surface explorer, J. Magn. Res. A 122 (1996) 104–109.
[5] B. Blümich, V. Anferov, S. Anferova, M. Klein, R. Fechete, M. Adams, F. Casanova, Simple NMR-mouse with a bar magnet, Concepts in Magnetic Resonance B 15 (2002) 255–261.
[6] J. Perlo, F. Casanova, B. Blümich, 3D imaging with a single sided sensor: An open tomograph, J. Magn. Res. 166 (2004) 228–235.
[7] M. Klein, R. Fechete, D.E. Demco, B. Blümich, Self-diffusion measurements by a constant relaxation method in strongly inhomogeneous magnetic fields, J. Magn. Res 164 (2003) 310–320.
[8] G. Guthausen, A. Guthausen, F. Balibanu, R. Eymael, K. Hailu, U. Schmitz, B. Blümich, Soft-matter analysis by the NMR-MOUSE, Macromol. Mater. Eng. 276/277 (2000) 25–37.
[9] R. Haken, B. Blümich, Anisotropy in tendon investigated in vivo by a portable NMR scanner, the NMR-MOUSE, J. Magn. Res. 144 (2000) 159–199.
[10] P.J. Prado, NMR hand-help moisture sensor, Magn. Res. Imag. 19 (2001) 505–508.
[11] K. Hailu, R. Fechete, D.E. Demco, B. Blümich, Segmental anisotropy in strained elastomers detected with a portable NMR scanner, Solid State Nucl. Magn. Res. 22 (2002) 343–347.
[12] S. Sharma, F. Casanova, W. Wache, A. Segre, B. Blümich, Analysis of historical porous building materials by the NMR-MOUSE, Magn. Res. Imag. 21 (2003) 249–255.
[13] P.J. Prado, Single sided imaging sensor, Magn. Res. Imag. 21 (2003) 300–397.
[14] Y.M. Pulyer, M.I. Hrovat, Generation of remote homogeneous magnetic fields, IEEE Trans. Magn. 38 (2002) 1553–1563.
[15] US Patent 6,489,872. E. Fukushima, J.A. Jackson, Unilateral magnet having a remote uniform field region for nuclear magnetic resonance.
[16] B. Luong, J.C. Goswami, A. Sezginer, D. Davies, Optimal control technique for magnet design in inside-out nuclear magnetic resonance, IEEE Trans. Magn. 37 (2001) 1015–1023.
[17] Y. Yao, C.S. Koh, D. Xie, Three-dimensional optimal shape design of magnetic pole in permanent magnet assembly for MRI taking account of eddy currents due to gradient coil field, IEEE Trans. Magn. 40 (2004) 1164–1167.
[18] S. Kakugawa, N. Hino, A. Komura, M. Kitamura, H. Takeshima, T. Yatsuo, H. Tazaki, Three-dimensional optimization of correction iron pieces for open high field MRI system, IEEE Trans. Magn. 14 (2004) 1624–1627.
[19] D.H. Kim, B.S. Kim, J.H. Lee, W.S. Nah, I.H. Park, 3-D optimal shape design of ferromagnetic pole in MRI magnet of open permanent magnet type, IEEE Trans. Appl. Superconduct. 12 (2002) 1467–1470.
[20] P.M. Glover, P.S. Aptaker, J.R. Bowler, E. Ciampi, P.J. McDonald, A novel high-gradient permanent magnet for the profiling of planar films and coatings, J. Magn. Res. 139 (1999) 90–97.
[21] A.E. Marble, I.V. Mastikhin, R.P. MacGregor, M. Akl, G. LaPlante, B.G. Colpitts, P. Lee-Sullivan, B.J. Balcom, Distortion free single point imaging of multi-layered composite sandwich panel structures, J. Magn. Res. 168 (2004) 164–174.
[22] P.T. Callaghan, Principles of Nuclear Magnetic Resonance Microscopy, Clarendon Press, New York, 1991.
[23] M.D. Hürlimann, Diffusion and relaxation effects in general stray field NMR experiments, J. Magn. Res. 148 (2001) 367–378.
[24] M.D. Hürlimann, D.D. Griffin, Spin dynamics of Carr–Purcell–Meiboom–Gill-like sequences in grossly inhomogeneous B_0 and B_1 fields and application to NMR well logging, J. Magn. Res. 143 (2000) 120–135.
[25] D. Eisenberg, W. Kauzmann, The Structure and Properties of Water, Oxford University Press, Oxford, 1969.
[26] J.A. Nelder, R. Mead, A simplex method for function minimization, Comput. J. 7 (1965) 308–313.